COMMUN. MATH. SCI.
Vol. 10, No. 3, pp. 875–888

A TWO TIME-SCALE MODEL FOR TIDAL BED-LOAD TRANSPORT*

STÉPHANE CORDIER†, CARINE LUCAS‡, AND JEAN DE DIEU ZABSONRÉ§

Abstract. The aim of this article is to derive a simplified sedimentation model thanks to an asymptotic analysis. We consider a two time scale erosion process due to tidal effects and we show that the approximation at the first order can model bed-load transport well. To this end, the simplified model is validated through numerical tests (evolution of a dune submitted to tidal effects in the ocean, run up near the coast) and compared to direct simulations that are very expensive in terms of computation time.

Key words. Shallow-Water Equations, bed-load transport, Exner equation, asymptotic developments, non-dimensional form, limit model, finite volumes scheme.

AMS subject classifications. 34E13, 74S10, 65M06.

1. Introduction

Developments in modeling and simulating bed-load transport are crucial to improve the prediction of water flow. Erosion phenomena such as transport or sedimentation can have a great impact on everyday life; one can cite mudslides due to rainfalls for example. Erosion is not only due to rain but it is also related to the oceans. Let us mention, e.g., scientific studies aim at limiting disappearance of sand, weakening coastal installations; see [1, 2]. Coastal erosion is linked to water flow, and to tides that increase the movements of the sea twice a day.

In this article, we consider models for the evolution of the topography in oceans, i.e. in shallow water submitted to tidal effects. More precisely, we study a Exner type equation for bed-load transport [5] coupled with Shallow-Water Equations. Several works have been done on such models; see for example [10, 15] for modeling issues and common empirical laws for the sediment discharge, [8, 12, 13] for stability analyses, or [6] for recent existence results.

The idea of the present work is to perform a multi-scale analysis in time for Shallow-Water Exner Equations and get a simplified system of equations satisfied by the first order approximation of our unknowns. We choose one of the simplest empirical expressions for the sediment discharge in the Exner Equation, namely the Grass model, since our goal is not to study the most complete model but to prove the validity of the proposed approach i.e. that a simplified model derived from multi-scale analysis can give qualitatively and quantitatively good approximations. This limit model is compared to the "reference solution", given by a finite volume scheme for the full model (which can be very intricate and computationally expensive); see [4]. The comparison between the two models shows that the solutions of the simplified model are rather accurate approximations of the reference solutions.

*Received: June 8, 2011; accepted (in revised version): November 6, 2011. Communicated by Francois Bouchut.
This work has been partially supported by the project METHODE 566 ANR-07-BLAN-0232.
†MAPMO UMR CNRS 7349, Université d'Orléans, Bâtiment de mathématiques, B.P. 6759 - 45067 Orléans cedex 2, France (cordier@math.cnrs.fr).
‡MAPMO UMR CNRS 7349, Université d'Orléans, Bâtiment de mathématiques, B.P. 6759 - 45067 Orléans cedex 2, France (carine.lucas@univ-orleans.fr).
§ISEA, Université Polytechnique de Bobo-Dioulasso, 01 B.P. 1091 Bobo 01, Burkina Faso (jzabsonre@gmail.com).

More precisely, the outline of the paper is the following: in Section 2, we explain the derivation of the equations. We start from Shallow-Water Equations that model the evolution of the fluid, and the classical Exner Equation for the evolution of the topography with Grass discharge. Then we introduce non-dimensional variables and parameters to get the scaled equations on which we perform the asymptotic analysis. The new simplified model is obtained by combining the first order terms of the asymptotic expansions. In Section 3, we explain the numerical methods used for the complete model and we compare the solutions of the two models. The first test case is a dune, initially at rest, whose shape oscillates with the tides. We also consider a beach test, that is a rectangular dune on an inclined plane. In order to validate the model, we study the numerical convergence of the limit model towards the complete model as the small parameter tends to zero. We complete this work with some tests on the numerical diffusion of the two models.

2. Derivation of the model

We begin our study with the derivation of the model: we consider the Shallow-Water Equations coupled with the Exner Equation for the evolution of the bed. We introduce non-dimensional variables in order to make an asymptotic analysis and obtain an approximate solution of the complete model.

2.1. Equations for bed-load transport. The first point is to write equations modelling the transport of sediments, in a shallow domain. Usually, the Shallow-Water Equations (SWE) are coupled with a transport equation on the sediment height. More precisely, we can define the following variables (see Figure 2.1):

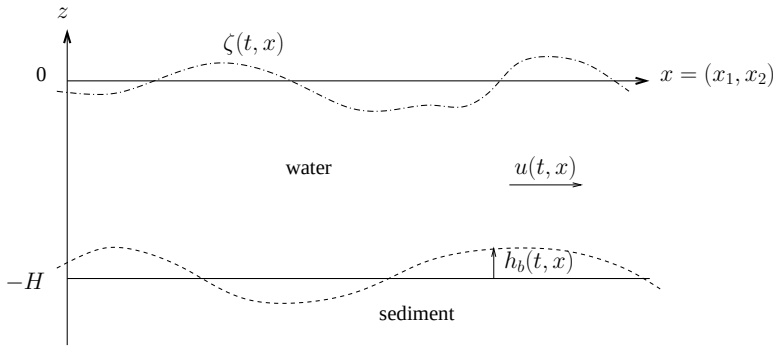

Fig. 2.1: Sediment layer and water with free surface

H is the mean water height on the domain, u the velocity of the fluid, and ζ is the function that describes the free surface. The function h_b denotes the sediment height starting from the level $z=-H$.

With these notations, the SWE are given by:

$$\partial_t(\zeta-h_b)+\operatorname{div}((\zeta+H-h_b)\,u)=0, \tag{2.1a}$$

$$\partial_t((\zeta+H-h_b)\,u)+\operatorname{div}((\zeta+H-h_b)\,u\otimes u) + g(\zeta+H-h_b)\nabla\zeta+f(\zeta+H-h_b)u^{\perp}=-ku, \tag{2.1b}$$

where g is the gravity, f the Coriolis term, k the friction coefficient, and $u^{\perp}={}^t(-u_2 \quad u_1)$ if u_1 and u_2 are the two components of the water velocity field u.

SWE (2.1) are coupled with an equation that describes the bed-load evolution. For the sediment transport, several empirical formulations of the classical Exner Equation [5] are given in the literature, depending on the sediment properties (see for example [14] and a review paper in preparation [9]). Let us only mention the Van Rijn [15] and Meyer-Peter and Müller [10] formulations for example. In this paper, for the sake of simplicity as explained in the introduction, we choose one of the simplest expression, namely the Grass model [7]:

$$\partial_t h_b + A\mathrm{div}(u^3) = 0, \tag{2.2}$$

where A is a coefficient given by the sediment characteristics (usually small).

In the following, our objective is to study the coupling between Equation (2.1) and (2.2).

2.2. Choice of the scalings: non-dimensional quantities. As we consider a domain such as an ocean, we have to take into account tidal effects. Then two length scales coexist, namely L (the tidal wave length) and l (the tidal excursion length). If σ denotes the tidal frequency and U the tidal current amplitude, we have $l = U/\sigma$. We introduce non-dimensional variables, with a prime, given by:

$$u = Uu',\ t = \frac{t'}{\sigma},\ x = lx',\ h_b = Hh_b',\ \zeta = \frac{UL\sigma}{g}\zeta'.$$

The scaling on ζ is linked to the typical momentum balance for a tidal wave.

We can introduce the small parameter δ, which is the ratio between l and L ($\delta \approx 10^{-3}$). This parameter δ can also be written as $\delta = U/(\sigma L)$, which means, considering the dispersion relation $L\sigma = \sqrt{gH}$, that the scaling on ζ reads:

$$\zeta = \delta H\zeta', \qquad \text{with} \quad \delta = \frac{l}{L} = \frac{U}{\sigma L}.$$

Finally, we define the non-dimensional parameters

$$A' = \frac{AU^3}{l\sigma H},\ f' = \frac{f}{\sigma},\ k' = \frac{k}{H\sigma}$$

to simplify the writing of the equations.

2.3. Non-dimensional equations. We replace the previous relations in equations (2.1)–(2.2); dropping the primes, we get the following non-dimensional relations:

$$\begin{aligned}
&\delta\partial_t\zeta - \partial_t h_b + \delta\mathrm{div}(\zeta u) + \mathrm{div}(u - h_b u) = 0,\\
&\partial_t\big((\delta\zeta + 1 - h_b)\,u\big) + \mathrm{div}\big((\delta\zeta + 1 - h_b)\,u\otimes u\big)\\
&\qquad\qquad + \frac{1}{\delta}(\delta\zeta + 1 - h_b)\nabla\zeta + f(\delta\zeta + 1 - h_b)\,u^{\perp} = -ku,\\
&\partial_t h_b + A\mathrm{div}(u^3) = 0.
\end{aligned}$$

As A is a small parameter (of order of δ^2), we can define a new time scale:

$$\tau = At,$$

and we assume h_b to be a function of τ and x only. Then we can rewrite the non-dimensional equations as:

$$\delta\partial_t\zeta+\delta A\partial_\tau\zeta-A\partial_\tau h_b+\delta\mathrm{div}(\zeta u)+\mathrm{div}(u-h_b u)=0, \tag{2.3a}$$

$$\partial_t\big((\delta\zeta+1-h_b)u\big)+A\partial_\tau\big((\delta\zeta+1-h_b)u\big)+\mathrm{div}\big((\delta\zeta+1-h_b)u\otimes u\big)+\frac{1}{\delta}(\delta\zeta+1-h_b)\nabla\zeta+f(\delta\zeta+1-h_b)u^\perp=-ku, \tag{2.3b}$$

$$\partial_\tau h_b+\mathrm{div}(u^3)=0. \tag{2.3c}$$

In order to study these relations, we perform an asymptotic development in powers of δ.

2.4. Asymptotic development. We decompose our variables in powers of δ:

$$\begin{aligned}\zeta&=\zeta^0+\delta\zeta^1+\delta^2\zeta^2\ldots,\\ h_b&=h_b^0+\delta h_b^1+\delta^2 h_b^2\ldots,\\ u&=u^0+\delta u^1+\delta^2 u^2\ldots.\end{aligned}$$

We replace these relations into Equation (2.3) and we identify the powers of δ. At the first order, we find:

$$\begin{aligned}&\mathrm{div}(u^0-h_b^0u^0)=0,\\ &\nabla\zeta^0=0,\\ &\partial_\tau h_b^0+\mathrm{div}\left(\left(u^0\right)^3\right)=0,\end{aligned}$$

and at the second order, we get the evolution of u^0:

$$\begin{aligned}&\partial_t\zeta^0+\mathrm{div}(\zeta^0u^0)+\mathrm{div}(u^1-h_b^1u^0-h_b^0u^1)=0,\\ &(1-h_b^0)\partial_t u^0+\mathrm{div}\left((1-h_b^0)u^0\otimes u^0\right)+(1-h_b^0)\nabla\zeta^1+f(1-h_b^0){u^0}^\perp=-ku^0,\\ &\partial_\tau h_b^1+3\mathrm{div}\left({u^0}^2u^1\right)=0.\end{aligned}$$

2.5. Model. The study of the first orders shows that ζ^0 is a function of t only, given by the boundary conditions. The evolutions of u^0 and h_b^0 satisfy

$$\mathrm{div}(u^0-h_b^0u^0)=0, \tag{2.4a}$$

$$\partial_\tau h_b^0+\mathrm{div}\left(\left(u^0\right)^3\right)=0, \tag{2.4b}$$

$$(1-h_b^0)\partial_t u^0+\mathrm{div}\left((1-h_b^0)u^0\otimes u^0\right)+(1-h_b^0)\nabla\zeta^1+f(1-h_b^0){u^0}^\perp=-ku^0, \tag{2.4c}$$

a system that can be solved using finite elements and the augmented Lagrangian method (in order to be able to treat the term in ζ^1).

REMARK 2.1. We could also introduce other space variables, namely $X=x/\delta$ and $\chi=\delta x$. In the first case, writing the equations, we find that the first order does not depend on X, and we get the same system as in Section 2.5 by taking the mean value, in X, of our equations.

In the second case, we obtain a system of the same type as the one of Section 2.5, but instead of $\nabla\zeta^1$ we have $\nabla\zeta^1+\nabla_\chi\zeta^0$, where ∇_χ is the gradient in the coordinates χ.

3. Numerical test

In order to validate our new model, we compare the results given by a finite volume scheme on the full equations (2.1)-(2.2) and the solution of (2.4) on a one dimensional test case. We consider a dune in the domain and we impose periodic boundary conditions on the velocity to simulate tides.

3.1. Finite volume scheme for the full model. The first approach is to get a "reference solution", through the resolution of the full Shallow-Water-Exner equations (2.1)–(2.2). This problem has been studied for example by [3, 4] using a finite volume scheme.
In order to keep the same notations as the one used in the above references, we do not consider notations of Figure 2.1 anymore but the one of Figure 3.1 (note that the variables are related through the relation $h = H + \zeta - h_b$).

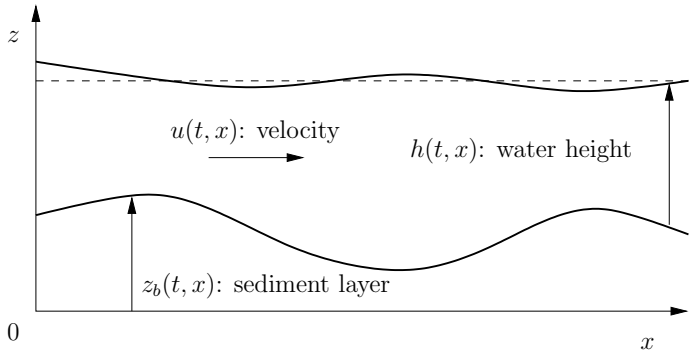

Fig. 3.1: Sediment layer and water with free surface for the finite volume scheme

With these notations, in one dimension (without the Coriolis term) and without friction ($k = 0$), Shallow-Water and Exner equations read:

$$\begin{aligned} &\partial_t h + \partial_x(hu) = 0, \\ &\partial_t(hu) + \partial_x(hu^2) + g(h + z_b)\partial_x h = 0, \\ &\partial_t z_b + A\partial_x u^3 = 0. \end{aligned} \tag{3.1}$$

System (3.1) can be written under the form $\partial_t W + A(W)\partial_x W = B(W)\partial_x W$, where $A(W) = \partial_W(F(W))$ is the Jacobian matrix of F, being

$$W = \begin{bmatrix} h \\ q \\ z_b \end{bmatrix}, \qquad F = \begin{bmatrix} q \\ \frac{q^2}{h} + \frac{1}{2}gh^2 \\ A\frac{q^3}{h^3} \end{bmatrix}, \qquad B = \begin{bmatrix} 0 & 0 & 0 \\ 0 & 0 & -gh \\ 0 & 0 & 0 \end{bmatrix}.$$

The full Shallow-Water Exner system (3.1) can also be written:

$$\partial_t W + \mathcal{A}(W)\partial_x W = 0, \tag{3.2}$$

where $\mathcal{A}(W) = A(W) - B(W)$. Due to the definition of F we have the following expression for $\mathcal{A}(W)$:

$$\mathcal{A}(W) = \begin{bmatrix} 0 & 1 & 0 \\ -\frac{q^2}{h^2} + gh & 2\frac{q}{h} & gh \\ -3A\frac{q^3}{h^4} & 3A\frac{q^2}{h^3} & 0 \end{bmatrix}.$$

To simulate this model, we consider the finite volumes scheme developed in [3]. Let W_i^n be the average of W over the volume V_i at time t^n. We obtain the following numerical scheme:

$$W_i^{n+1} = W_i^n - \frac{dt}{dx}\left(\mathcal{D}^+_{i+1/2} + \mathcal{D}^-_{i+1/2}\right),$$

with

$$\begin{aligned}\mathcal{D}^\pm_{i+1/2} = &\pm\frac{\alpha_0}{2}(W^n_{i+1} - W^n_i)\\ &\pm\left(\frac{1}{2}+\frac{\alpha_1}{2}\right)\left(F(W^n_{i+1}) - F(W^n_i) - B_{i+1/2}(W^n_{i+1} - W^n_i)\right)\\ &\pm\frac{\alpha_2}{2}\mathcal{A}_{i+1/2}\left(F(W^n_{i+1}) - F(W^n_i) - B_{i+1/2}(W^n_{i+1} - W^n_i)\right),\end{aligned}$$

where $\mathcal{A}_{i+1/2}$ is the Roe linearization matrix. The coefficients α_i are given by the formulas:

$$\begin{aligned}\alpha_0 &= \frac{|\lambda_1|\lambda_2\lambda_3}{(\lambda_2-\lambda_1)(\lambda_3-\lambda_1)} + \frac{|\lambda_2|\lambda_1\lambda_3}{(\lambda_1-\lambda_2)(\lambda_3-\lambda_2)} + \frac{|\lambda_3|\lambda_1\lambda_2}{(\lambda_3-\lambda_1)(\lambda_3-\lambda_2)},\\ \alpha_1 &= -\lambda_1\left(\frac{|\lambda_2|}{(\lambda_1-\lambda_2)(\lambda_3-\lambda_2)} + \frac{|\lambda_3|}{(\lambda_1-\lambda_3)(\lambda_2-\lambda_3)}\right)\\ &\quad -\lambda_2\left(\frac{|\lambda_1|}{(\lambda_2-\lambda_1)(\lambda_3-\lambda_1)} + \frac{|\lambda_3|}{(\lambda_1-\lambda_3)(\lambda_2-\lambda_3)}\right)\\ &\quad -\lambda_3\left(\frac{|\lambda_1|}{(\lambda_2-\lambda_1)(\lambda_3-\lambda_1)} + \frac{|\lambda_2|}{(\lambda_3-\lambda_2)(\lambda_1-\lambda_2)}\right),\end{aligned}$$

and

$$\alpha_2 = \frac{|\lambda_1|}{(\lambda_2-\lambda_1)(\lambda_3-\lambda_1)} + \frac{|\lambda_2|}{(\lambda_1-\lambda_2)(\lambda_3-\lambda_2)} + \frac{|\lambda_3|}{(\lambda_3-\lambda_1)(\lambda_3-\lambda_2)},$$

where the coefficients λ_i (for $i=0,1,2$) are the eigenvalues of the matrix $\mathcal{A}_{i+1/2}$; see [4].

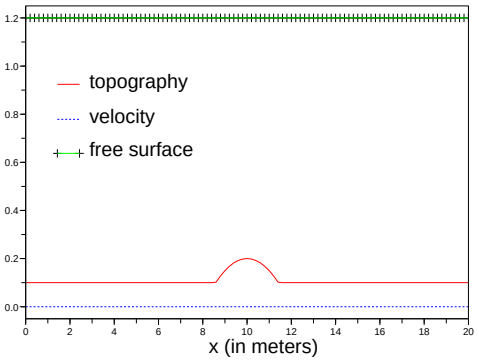

Fig. 3.2: Initial conditions

3.2. Numerical results. We consider the spatial domain $[0,20]$, discretized with 100 points. In this domain, we impose an initial dune, given by

$$z_b(t=0,x) = b_0 + \max\left(0.1 - 0.05(x-10)^2, 0\right), \quad \text{with } b_0 = 0.1;$$

see Figure 3.2.

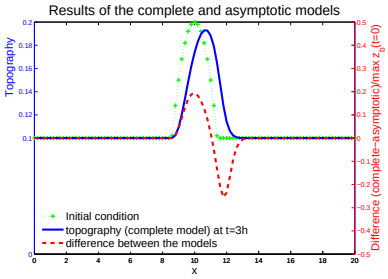

(a) $t = 3$ h.

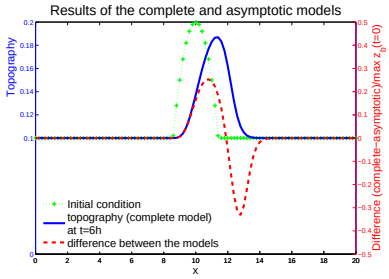

(b) $t = 6$ h.

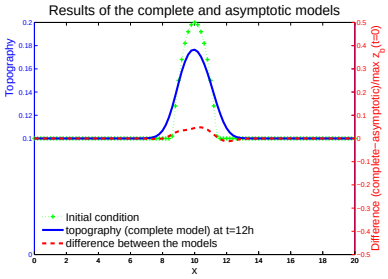

(c) $t = 12$ h.

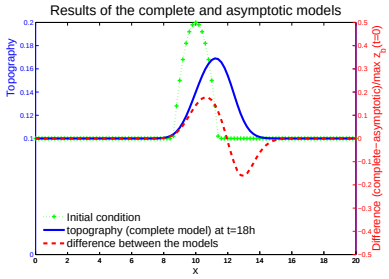

(d) $t = 18$ h.

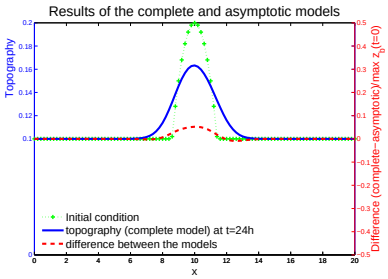

(e) $t = 24$ h.

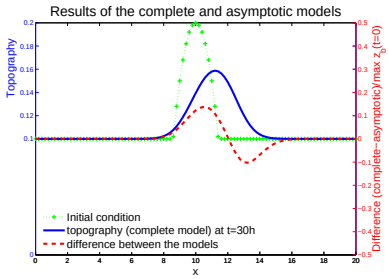

(f) $t = 30$ h.

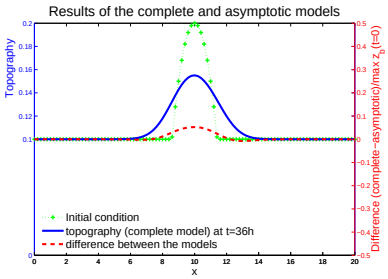

(g) $t = 36$ h.

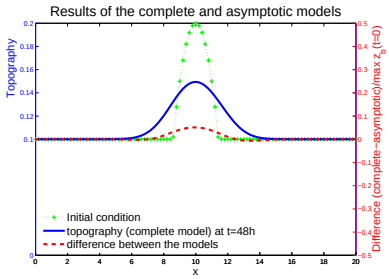

(h) $t = 48$ h.

Fig. 3.3: Evolution of the topography with 100 points

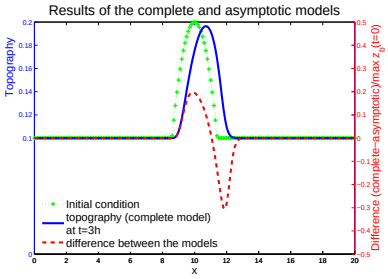

(a) $t = 3$ h.

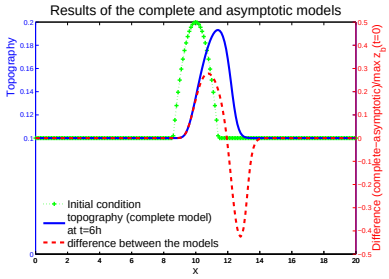

(b) $t = 6$ h.

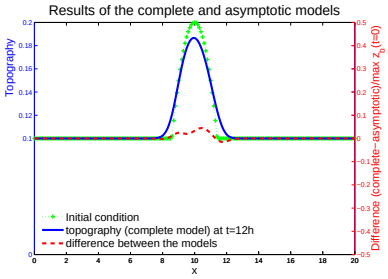

(c) $t = 12$ h.

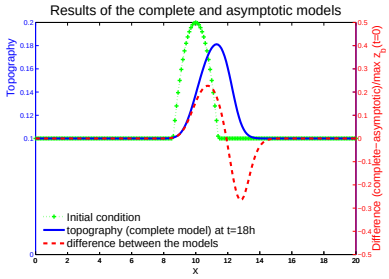

(d) $t = 18$ h.

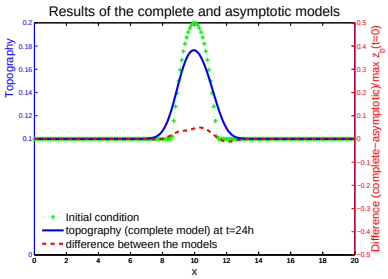

(e) $t = 24$ h.

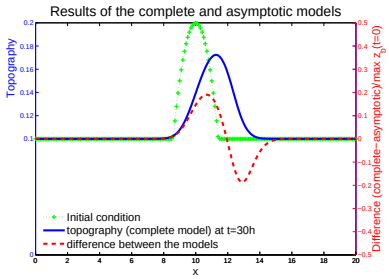

(f) $t = 30$ h.

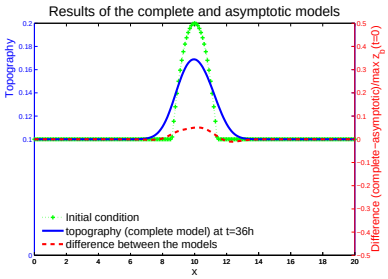

(g) $t = 36$ h.

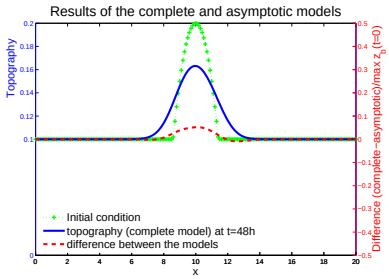

(h) $t = 48$ h.

Fig. 3.4: Evolution of the topography with 200 points

In order to have a constant free surface, we choose a low velocity with periodic condition on the boundaries $x=0$ and $x=20$, namely:

$$u(t,x=0)=u(t,x=20)=5.4\sin(\pi t/6), \quad \text{in m/h.}$$

The variable t is the time expressed in hours, such that there are two periods a day ($\sigma \approx 2.315\times 10^{-5}$ s^{-1}). We assume that at the initial time, the velocity is null, $u(t=0,x)=0$, such that the initial conditions are given by Figure 3.2. For these choices of initial conditions and velocity, the value of δ is 0.0002 and the free surface stays flat without moving.

Let us explain the results we obtained. We present the evolution of the bottom at the times $t=3$, 6, 12, 18, 24, 30, 36, and 48 hours respectively in Figure 3.3 (blue continuous line), for the solution of System (3.1) with $A=0.001$ and 100 points. In Figure 3.4, we used a finer grid and divided the space step by 2 to confirm and improve the results. One can first notice that the dune is moving towards the right or the left, depending on the sign of the velocity. Thanks to the mesh refinement, we can assert that the displacement of the dune cannot be attributed solely to numerical diffusion. At the same time, the dune is spreading.

Let us now compare the solutions of the two systems. One may know that for 100 points, the complete model needs nearly one hour; with 200 points, the computation time is several hours, whereas the limit model takes a few seconds. In Figure 3.3, the red dashed line gives the difference between the complete and the limit model, rescaled by the maximum of the initial topography (*i.e.* 0.2 m). We first conclude that our new simplified system gives good results on long time and the computation time is much smaller than for the complete model. However, when the top of the dune is not at $x=10$ m, i.e. when the dune is slightly shifted, we observe important local errors on the slopes.

To improve the comparison between the two models (full Shallow-Water system with Exner equation and the simplified limit model), we consider the two following functions (of time):

$$Z(t)=\max_{0\le x\le L} z_b(x,t) \quad \text{and} \quad N(t)=\text{card}\left\{ i \text{ s.t. } z_b(x_i,t)\ge \frac{Z(t)-b_0}{2}+b_0 \right\}.$$

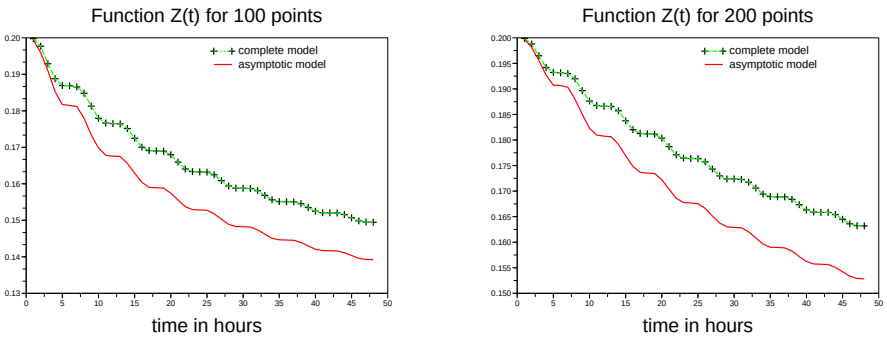

(a) 100 points. (b) 200 points.

Fig. 3.5: Graphs of the function $Z(t)$

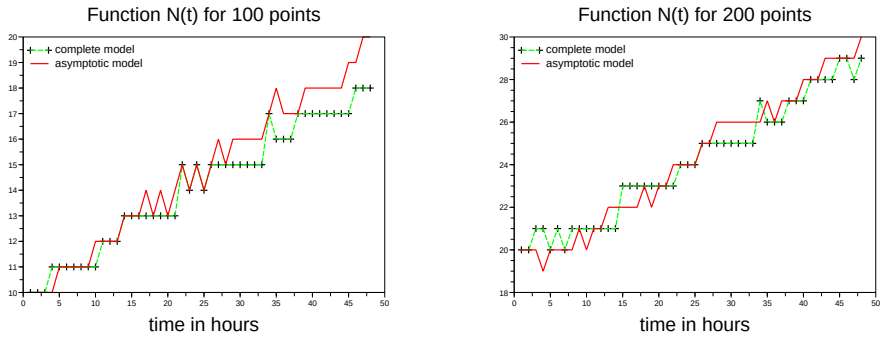

(a) 100 points. (b) 200 points.

Fig. 3.6: Graphs of the function $N(t)$

The function Z represents the evolution in time of the maximum of the dune, and the function N characterize the spread of the dune. The results are plotted in Figures 3.5-3.6 (the sawtooth shape of the function N is due to the integer values of $N(t)$ and to the discrete values of the time, every one hour).

The first conclusion we can give with these numerical results is that the simplified limit model behaves very well compared to the complete model but has the advantage of a lower computation time.

3.3. More numerical results.

3.3.1. Beach test. We improve the numerical results with the simulation of a run up in the spirit of [4] but in which we add the effects of tides. In this test, a 15 m long channel has a small slope (0.052%) with a rectangular sand layer of 4.5 cm between 4.5 m and 9 m (see Figure 3.7). This is a way to model the phenomenon of beach erosion.

In Figure 3.8 we plotted the results of the models on this beach test, namely we give the solution of the complete model (3.1) (blue continuous line) and the difference between the two models normalized by the maximum of the initial topography (red dashed line). The error is mainly located on the slopes of the dune and stays quite small.

This shows that the asymptotic model is a good approximation of the complete model for the beach test case also.

3.3.2. Convergence of the asymptotic model. The analytic proof of the convergence of the asymptotic model towards the complete model is beyond the scope of this paper. But we can study the limit of the asymptotic model as δ tends to zero from a numerical point of view. To this end, we compute the norms of the difference between the results of the two models at $t = 48$ h, for 100 and 200 points, for various values of δ. The configuration is the dune of Section 3.2 and $\delta_0 = 0.0002$ the value corresponding to the conditions pointed out in that part. The results are plotted in Figure 3.9. We see that, as δ tends to zero, the errors are of order 1 in δ, as we assumed when we wrote the asymptotic model. These results show that our assumptions are satisfied from a numerical point of view.

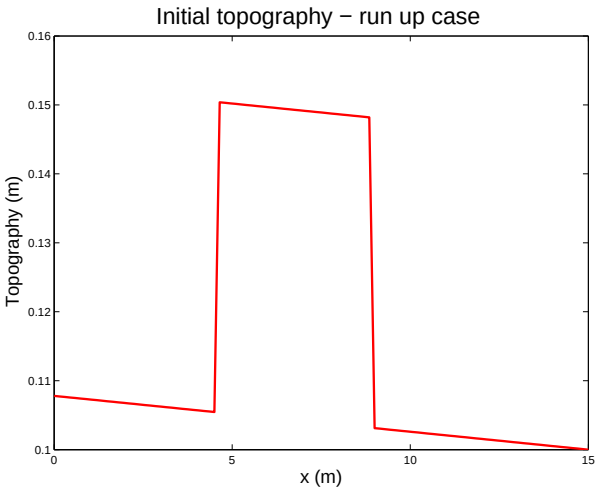

Fig. 3.7: Initial conditions for the beach test

3.3.3. Numerical diffusion. In this part, we focus our attention on the spreading on the dune, in both models. To that end, we consider several space steps: $dx = 0.2$ m, $\frac{dx}{2}$, $\frac{dx}{4}$, and $\frac{dx}{8}$. Our goal is to quantify the effects of the numerical diffusion.

In Figures 3.10-3.11, we plotted the functions Z and N for the various space steps, for the complete and the limit models. (The functions N are rescaled to take into account the number of points.) As explained before, the two models have the same behavior, although this is not the point we want to emphasize. These figures and Figures 3.3-3.4 show that the x-coordinate of the culmination of the dune does not depend on the space step (the movement due to tides is well reproduced by the two models). However, in both cases, the height of the culmination point is linked to the value of the space step: the diffusion that makes the dune spread is only *numerical diffusion*, even if it seems "natural". This means that the diffusion of the topography is not taken into account in the complete system (2.1)-(2.2) (and consequently in the limit model).

4. Conclusions

In this paper, we performed asymptotic expansions in order to decouple the two time scales that appear in oceans, considering the effect of tides. We obtained a new model and we carried out some experiments. Comparisons with the complete model give good results in one dimension, with the advantage that our new limit model is much faster (a few seconds compared to a few hours) and easier to implement than the complete one.

However, the spreading of the dune is only due to the numerical diffusion, which means that, in the Shallow-Water system with Exner equation considering Grass flow, there is no diffusion of the evolution of the topography. This is contrary to the observations one can make, and we can suggest to add *diffusive terms* in the Exner equation, as in [16] for example, or [11] for the Meyer-Peter and Müller equation.

The numerical validation of these results for the two dimensional case is still in progress.

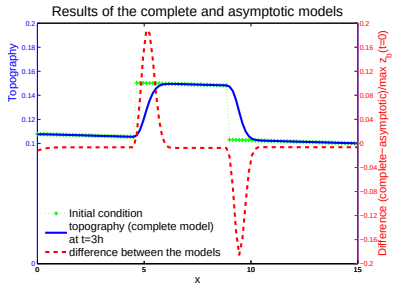

(a) $t = 3$ h.

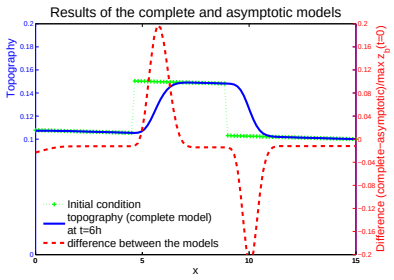

(b) $t = 6$ h.

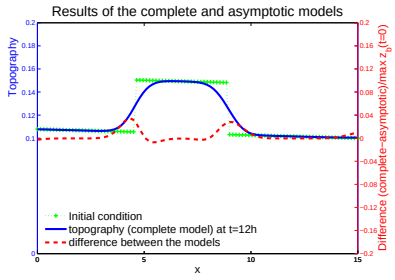

(c) $t = 12$ h.

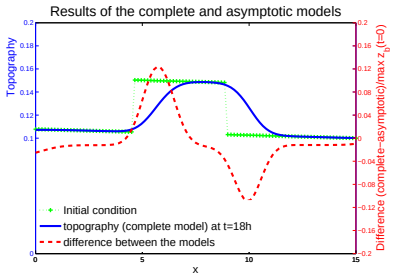

(d) $t = 18$ h.

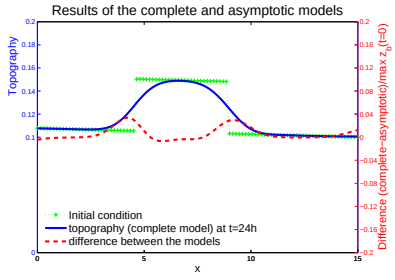

(e) $t = 24$ h.

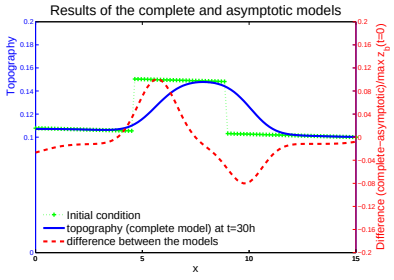

(f) $t = 30$ h.

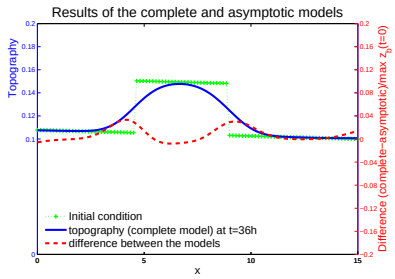

(g) $t = 36$ h.

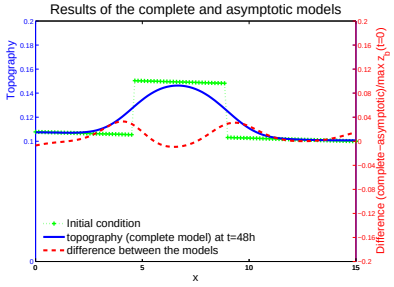

(h) $t = 48$ h.

Fig. 3.8: Evolution of the topography in the beach test case with 100 points

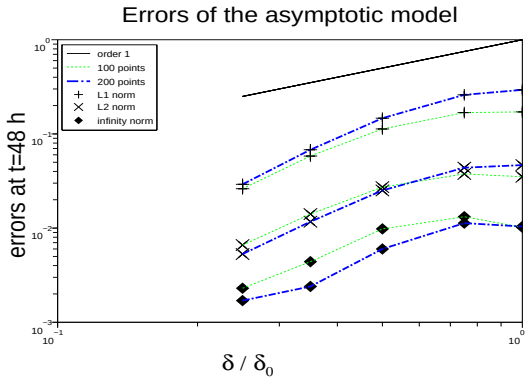

Fig. 3.9: Errors of the asymptotic model for 100 and 200 points

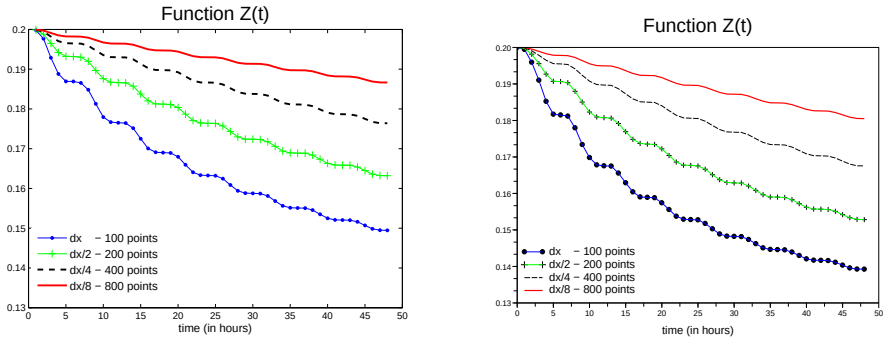

(a) Complete model. (b) Limit model.

Fig. 3.10: Graphs of the functions $Z(t)$

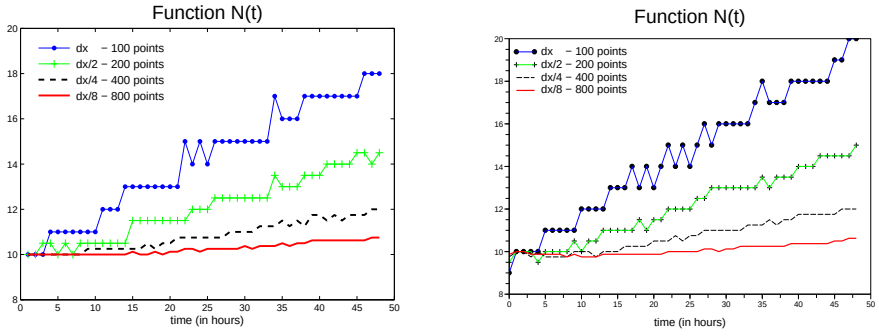

(a) Complete model. (b) Limit model.

Fig. 3.11: Graphs of the functions $N(t)$

Acknowledgments. As this work started with a French-American collaboration, the second author would like to thanks the "Equipes Associées" program of INRIA (between J. McWilliams's team (UCLA) and Moise INRIA team (Grenoble, France), directed by E. Blayo) which partly funded this work.

The third author is partially supported by the AUF, and is very grateful to the MAPMO laboratory for the accommodation he received.

The authors would like to thank the anonymous referee for his numerous suggestions and constructive comments.

REFERENCES

[1] P. Azerad, F. Bouchette, D. Isebe, and B. Mohammadi, *Shape optimization of geotextile tubes for sandy beach protection*, Int. J. Num. Meth. Eng., 74, 1262–1277, 2008.

[2] A. Bouharguane and B. Mohammadi, *Minimization principles for the evolution of a soft sea bed interacting with a shallow sea*, submitted.

[3] J.M. Castro and E.D. Fernández-Nieto, *A class of computationally fast first order finite volume solvers. PVM Methods*, SIAM J. Sci. Comput., submitted.

[4] J.M. Castro, E.D. Fernández-Nieto, and A. Ferreiro, *Sediment transport models in Shallow Water*, Computers & Fluids, 37(3), 299–316, 2008.

[5] F. Exner, *Uber die wechselwirkung zwischen wasser und geschiebe in flussen*, Sitzber., Akad. Wiss Wien, Part IIa, Bd., 134, 1925.

[6] I. Faye, E. Frenod, and D. Seck, *Singularly perturbed degenerated parabolic equations and application to seabed morphodynamics in tided environment*, Disc. Cont. Dyn. Sys.: Series A, 29(3), 1001–1030, 2011.

[7] A.J. Grass, *Sediment transport by waves and currents*, Technol. Report No.: FL29, SERC London, Cent. Mar., 1981.

[8] S. Hulscher, *Formation and Migration of Large-Scale, Rhythmic Sea-Bed Patterns: A Stability Approach*, Ph.D. thesis, Utrecht University, 1996.

[9] M.H. Le, B. Cheviron, O. Cerdan, S. Cordier, and P. Sochala, *A review of physically based modeling of soil erosion by water*, preprint, 2011.

[10] E. Meyer-Peter and R. Müller, *Formulas for bed-load transport*, Proceedings of the second meeting of the International Association for Hydraulic Structures Research, Stockholm: 39–64, 1948.

[11] T. Morales de Luna, M.J. Castro Díaz, and C. Parés Madroñal, *A duality method for sediment transport based on a modified Meyer-Peter & Müller model*, J. Sci. Comput., 48(1-3), 258–273, 2011.

[12] P.C. Roos, *Seabed Pattern Dynamics and Offshore Sand Extraction*, Ph.D. thesis, University of Twente, 2004.

[13] H. Schuttelaars, *Evolution and Stability Analysis of Bottom Patterns in Tidal Embayements*, Ph.D. thesis, Utrecht University, 1997.

[14] R. Soulsby, *Dynamics of Marine Sands: A Manual for Practical Applications*, Thomas Telford, London, 1997.

[15] L. Van-Rijn, *Sediment transport, Part 1: Bed load transport*, J. Hyd. Eng., 110(10), 1431–1456, 1984.

[16] J. de D. Zabsonré, C. Lucas, and E. Fernández-Nieto, *An energetically consistent viscous sedimentation model*, Math. Model. Meth. Appl. Sci., 19(3), 477–499, 2009.